united nations
educational, scientific
and cultural
organization

international atomic
energy agency

the
abdus salam
international centre for theoretical physics

SMR 1521/3

AUTUMN COLLEGE ON PLASMA PHYSICS

13 October - 7 November 2003

Variational Principles

D. C. Montgomery

Dartmouth College,
Dept. of Physics and Astronomy
Hanover, USA

These are preliminary lecture notes, intended only for distribution to participants.

VARIATIONAL PRINCIPLES:

WHAT CAN THEY TELL US ABOUT PLASMA STEADY STATES?

PROTOTYPE IS TAYLOR'S CALCULATION OF REVERSED-FIELD PINCH BEHAVIOR.

→ ENERGY DECAYS, MOSTLY RESISTIVELY (?)

→ MAGNETIC HELICITY IS CONSERVED.

→ $\underset{\sim}{v} \cong 0$.

$\Longrightarrow \quad \nabla \times \underset{\sim}{B} = \lambda \underset{\sim}{B}$,

AN APPROXIMATELY FORCE-FREE, STEADY STATE : $\underset{\sim}{j} \times \underset{\sim}{B} = 0$.

NO CONFINEMENT, IF $\underset{\sim}{j}_{\perp} \times \underset{\sim}{B} \cong \nabla p$.

DOES NOT OBEY OHM'S LAW:

$\nabla \times \underset{\sim}{j} \neq 0$ (DOES $\underset{\sim}{j} = \sigma \underset{\sim}{E}$?)

Given a non-uniform, rigid conductor

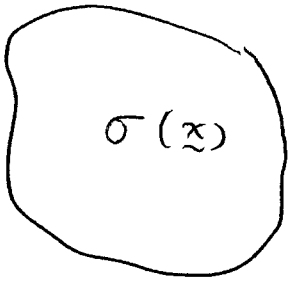

with spatially non-uniform conductivity $\sigma(\underset{\sim}{x})$.

Hold the surface at a fixed potential, which may also depend on space: $\Phi_s(\underset{\sim}{x})$.

What current flows, if it is allowed to enter and leave the surface at will?

$$\underset{\sim}{j} = \sigma \underset{\sim}{E} = -\sigma \nabla \Phi \quad \text{(steady state)}$$

$$\nabla \cdot \underset{\sim}{j} = 0 \quad \left(\text{continuity, } \frac{\partial}{\partial t} = 0\right)$$

$$\therefore \boxed{\nabla \cdot (\sigma \nabla \Phi) = 0}$$

+ boundary condition (Dirichlet)

Minimize Ohmic dissipation, subject to boundary condition (a constraint).

$$\text{Dissipation} = \frac{1}{2}\int_V \sigma(\nabla\Phi)\,d^3x \equiv \mathcal{L}$$

$$\delta\mathcal{L} = \int \sigma\nabla\Phi\cdot\nabla\delta\Phi\,d^3x$$

$$= \int_{\text{Surface}} \hat{n}\,dA\cdot\delta\Phi\nabla\Phi - \int d^3x\,\delta\Phi\,\nabla\cdot(\sigma\nabla\Phi)$$

$\delta\Phi \to 0$

$$\delta\mathcal{L} = 0 \iff \boxed{\nabla\cdot(\sigma\nabla\Phi) = 0}$$

THAT CURRENT DENSITY $\underset{\sim}{j}(\underset{\sim}{x})$ DEVELOPS WHICH WILL MINIMIZE THE OVERALL OHMIC DISSIPATION, SUBJECT TO BOUNDARY CONDITIONS.

(KIRCHOFF, 1848)

NAVIER-STOKES SHEAR FLOW

BETWEEN INFINITE, PARALLEL PLANES

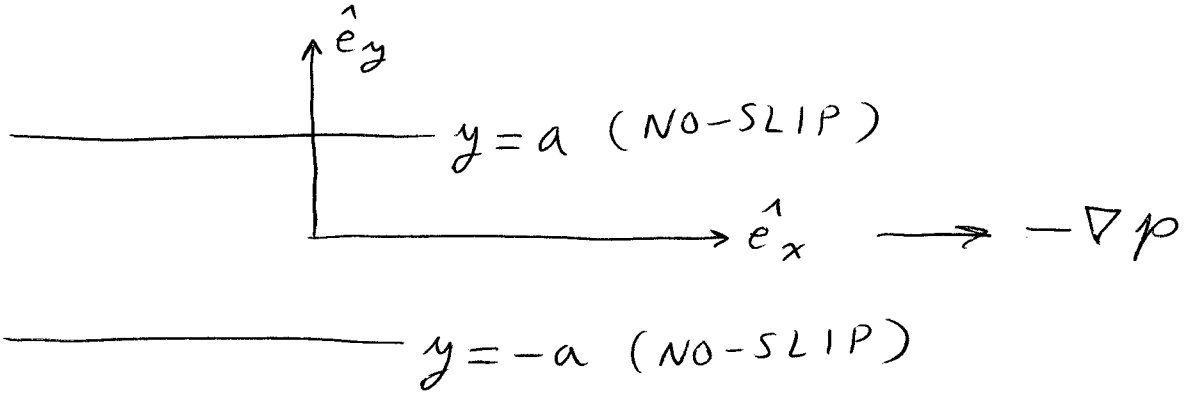

$$\frac{\partial}{\partial z}=0,\quad \frac{\partial}{\partial t}=0,\quad \frac{\partial}{\partial x}=0 \quad \text{(symmetries)}$$

$$\mathcal{D} = \text{Dissipation} = \rho\frac{\nu}{2}\int(\nabla\times\underset{\sim}{v})\,d^3x = \frac{\rho\nu}{2}\int\underset{\sim}{\omega}^2 d^3x$$

Assume $\underset{\sim}{v} = u(y)\hat{e}_x$

$$\mathcal{D} \longrightarrow \frac{\rho\nu}{2}\int d^3x\left(\frac{du(y)}{dy}\right)^2$$

$\mathcal{F}$ = Flow rate = const. $= \left(\int u(y)\,d^3x\right)\rho$

is constraint.

USE LAGRANGE MULTIPLIER

$$\delta(\mathcal{D}+\alpha\mathcal{F})=0$$

$$\delta \mathcal{H} = \rho \nu \int_{-a}^{a} \frac{du}{dy} \frac{d}{dy} \delta u \; d^3x$$

$$= - \int \rho \nu \frac{d^2 u}{dy^2} \delta u \; d^3x \qquad (\delta u = 0 \text{ at } y = \pm a; \text{ periodic in } x, z)$$

Euler-LaGrange Eq.

$$\nu \frac{d^2 u(y)}{dy^2} + \alpha = 0$$

$$u(y) = -\frac{\alpha}{2\nu} y^2 + c_1 y + c_2$$

Determine c_1, c_2 by $u(\pm a) = 0$:

$$\boxed{u(y) = \frac{\alpha}{2\nu} (a^2 - y^2)}$$

Plane Poiseuille flow

PROFILE IS GIVEN BY STATE OF MINIMUM RATE OF ENERGY DISSIPATION, SUBJECT TO CONSTRAINTS.

SAME IS TRUE FOR OTHER 1D SHEAR FLOWS (PLANE COUETTE FLOW, PIPE FLOW, ROTATING COUETTE FLOW.

"MINIMUM ENERGY DISSIPATION RATE"

A PRINCIPLE WHICH PREDICTS BASIC LAMINAR STATES WHICH ARE BOTH STEADILY DRIVEN AND DISSIPATIVE, IN

(1) HYDRODYNAMICS

(2) ELECTRIC CIRCUITS WITH NON-UNIFORM RESISTANCES.

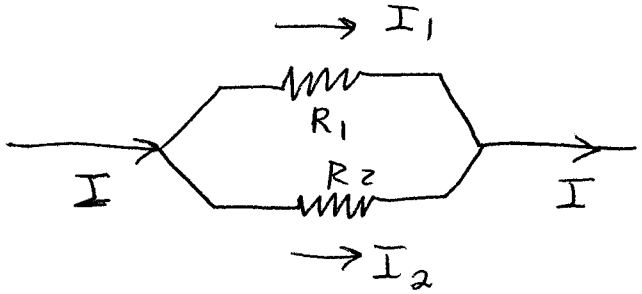

$$I_1^2 R_1 + I_2^2 R_2 = \text{DISSIPATION RATE}$$

$$I_1 + I_2 = I = \text{CONSTANT} \quad (\text{CONSTRAINT})$$

$$\alpha + I_1 R_1)\delta I_1 + (\alpha + I_2 R_2)\delta I_2 = 0$$

$$\left.\begin{aligned} \alpha + I_1 R_1 &= 0 \\ \alpha + I_2 R_2 &= 0 \end{aligned}\right\} \Rightarrow \quad I_1 R_1 = I_2 R_2$$

$$I_1 \left(1 + \frac{R_1}{R_2}\right) = I$$

$$I_1 = \frac{R_2 I}{R_1 + R_2}, \quad I_2 = \frac{R_1 I}{R_1 + R_2}$$

NOTE THAT THIS IS ALSO STATE OF MINIMUM RATE OF ENTROPY PRODUCTION, BUT ONLY IF THE TWO RESISTORS ARE AT THE SAME TEMPERATURE, T.

$$\frac{I_1^2 R_1}{T} + \frac{I_2^2 R_2}{T} = \frac{dQ/dt}{T} = \text{ENTROPY PRODUCTION RATE}$$

$\Rightarrow$ HOWEVER, IF TWO RESISTORS ARE HELD AT DIFFERENT TEMPERATURES,

MINIMIZING THE ENTROPY PRODUCTION RATE,

$$\frac{I_1^2 R_1}{T_1} + \frac{I_2^2 R_2}{T_2} = \sum \frac{dQ/dt}{T}$$

DOES <u>NOT</u> GIVE THE RIGHT ANSWER.

MINIMUM RATE OF ENERGY DISSIPATION SEEMS MORE FUNDAMENTAL THAN MINIMUM RATE OF ENTROPY PRODUCTION.

WHAT IS THE PHYSICAL BASIS OF THE TENDENCY TOWARD MINIMUM DISSIPATION?

$\Longrightarrow$ CONJECTURE: PHYSICAL SYSTEMS WANT TO RELAX TO THERMAL EQUILIBRIUM WHICH IS SPATIALLY UNIFORM. IF THEY ARE PROPPED AWAY FROM UNIFORMITY BY BOUNDARY CONDITIONS ("FORCING"), THEY WILL GET AS CLOSE TO THE UNIFORM STATE AS THEY CAN.

$\Longrightarrow$ "MINIMUM DISSIPATION RATE" IS BASICALLY A PRINCIPLE OF MAXIMUM SMOOTHNESS.

$$\text{OHMIC DISSIPATION} = \int \eta \underset{\sim}{j}\, d^3x, \quad \propto \int \eta (\nabla \times \underset{\sim}{B})^2 d^3x \qquad (\nabla \cdot \underset{\sim}{B} = 0)$$

$$\text{VISCOUS DISSIPATION} = \rho \int \nu (\nabla \times \underset{\sim}{v})^2 d^3 = \rho \int \nu \underset{\sim}{\omega}^2 d^3x \qquad (\nabla \cdot \underset{\sim}{v} = 0)$$

THESE ARE THE NATURAL MEASURES OF THE DEGREE OF NONUNIFORMITY OF $\underset{\sim}{B}, \underset{\sim}{v}$.

FOURIER HEAT CONDUCTION PRESENTS DIFFICULTIES

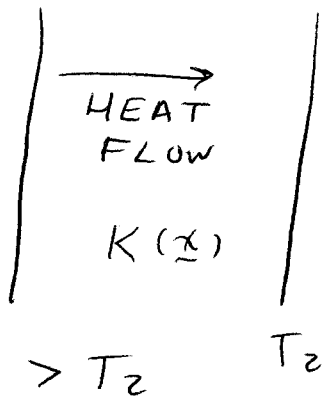

PLATES BOUND A REGION OF VARIABLE THERMAL CONDUCTIVITY $K(\underset{\sim}{x})$

HEAT CURRENT $= -K\nabla T = \underset{\sim}{J}$

$$\nabla \cdot \underset{\sim}{J} = 0 \Rightarrow \nabla \cdot (K \nabla T) = 0$$

for steady state

QUANTITY TO BE VARIED IS, CLEARLY,

$$\mathcal{U} = \int_V K(\nabla T)^2 d^3x$$

$$\delta \mathcal{U} = 0 \Rightarrow \nabla \cdot (K \nabla T) = 0$$

$\mathcal{U}$ is a measure of smoothness of T, but not in any meaningful sense a rate of entropy production.

FOR MHD, TRY TO MINIMIZE

$$\int (\eta \underset{\sim}{j}^2 + \nu \underset{\sim}{\omega}^2) d^3x$$

ASSUMING UNIFORM TEMPERATURE
(INFINITE THERMAL CONDUCTIVITY).

CYLINDER OF UNIFORM MAGNETOFLUID.

IMBEDDED DC MAGNETIC FIELD (AXIAL).

APPLIED POTENTIAL DROP FROM END TO END
(MEAN DC ELECTRIC FIELD).

Montgomery and Phillips
Phys. Rev. A 38, 2953 (1988).

Montgomery, Phillips, and Theobald
Phys. Rev. A 40, 1515 (1989).

CRUCIAL TO THE RESULTS
ARE CONSTRAINTS AND
BOUNDARY CONDITIONS.

A full set of boundary conditions at a material wall:

Perfect conductor: $\underset{\sim}{B} \cdot \hat{n} = 0$

$\underset{\sim}{j} \times \hat{n} = 0$

Perfect conductor with thin layer of insulator: $\underset{\sim}{B} \cdot \hat{n} = 0$

$\underset{\sim}{j} \cdot \hat{n} = 0$

No-slip mechanical wall: $\underset{\sim}{v} = 0$

Stress-free mechanical wall:

$\underset{\sim}{v} \cdot \hat{n} = 0$

$\hat{n} \times \underset{\approx}{\sigma} \cdot \hat{n} = 0$

$\underset{\approx}{\sigma}$ = viscous stress tensor

Sometimes we settle for $\underset{\sim}{v} \cdot \hat{n} = 0$

$\nabla \times \underset{\sim}{v} \cdot \hat{n} = \underset{\sim}{\omega} \cdot \hat{n} = 0$

(implied by, but does not imply, no-slip wall)

APART FROM KINEMATICAL CONSTRAINTS IMPOSED BY THE BOUNDARY CONDITIONS (SUCH AS FLUX CONSERVATION), MONTGOMERY and PHILLIPS WERE ABLE TO PROVE ONLY ONE DYNAMICAL CONSTANT OF THE MOTION FOR THE ELECTRICALLY-DRIVEN PERIODIC CONDUCTING CYLINDER: THE RATE OF SUPPLY AND DISSIPATION OF MAGNETIC HELICITY:

$$2\eta \int \underset{\sim}{j} \cdot \underset{\sim}{B}\, d^3x = 2E_0 \pi a^2 L_z B_0 .$$

MINIMIZING ENERGY DISSIPATION WITH RESPECT TO THIS AND THE BOUNDARY-CONDITION IMPLIED CONSTANTS, ASSUMING $\underset{\sim}{v} = 0$, GIVES THE EULER-LAGRANGE EQUATION,

$$\nabla \times \underset{\sim}{j} + \alpha \underset{\sim}{j} + \nabla S = 0$$

$$\nabla^2 S = 0$$

nonvanishing β_{nmq} are the β_{00q}, which are straightforwardly obtained from setting the z component of $j_{00q}=0$ at $r=a$,

$$\beta_{00q}=-\zeta_{00q}\lambda_{00q}^3 J_0(\lambda_{00q}a)\ . \tag{4.10}$$

There are two possible signs of $\lambda_{nmq}=\pm(\gamma_{nmq}^2+k_n^2)^{1/2}$ for each $\gamma_{nmq}>0$. It will be seen in Sec. V that the sign of λ_{nmq} is fixed by the sign of $\langle \mathbf{j}\cdot\mathbf{B}\rangle$. The γ_{nmq} are ordered in q as ascending positive values, with $q=1$ always identifying the lowest nonzero γ_{nmq} for any n and m.

The determination of the possible $\mathbf{j}_{nmq}$ which satisfy all the boundary conditions is now complete, up to the overall multiplicative amplitude ζ_{nmq}. The constraint of constant helicity supply rate will be expressed as $\langle \mathbf{j}_{nmq}\cdot\mathbf{B}_{nmq}\rangle=$const where $\mathbf{B}_{nmq}$ is the magnetic field to be determined in Sec. V.

V. ASSOCIATED MAGNETIC FIELD PROFILES

For each $\mathbf{j}_{nmq}$ of the form of Eq. (4.1), there is a $\mathbf{B}_{nmq}$ for which

$$\nabla\times\mathbf{B}_{nmq}=\mathbf{j}_{nmq}=\mathbf{J}_{nmq}+\frac{\nabla s_{nmq}}{\lambda_{nmq}}\ . \tag{5.1}$$

It is useful to write ∇s_{nmq} in the form of Eq. (4.4b) and identify

$$\mathbf{B}_{nmq}=\frac{\zeta_{nmq}\mathbf{J}_{nmq}}{\lambda_{nmq}}+\mathbf{B}_0+\nabla\chi_{nmq}+\begin{cases}(d_{nmq}/ik_n)\nabla\times\hat{\mathbf{e}}_z I_m(k_n r)e^{i(m\varphi+k_n z)} \\ -id_{0mq}\hat{\mathbf{e}}_z r^m e^{im\varphi}\end{cases}\ \text{for}\ \begin{cases}n\neq 0\\ n=0\end{cases}$$
$$+\frac{\beta_{00q}r}{2\lambda_{00q}}\delta_{n,0}\delta_{m,0}\hat{\mathbf{e}}_\varphi\ , \tag{5.2}$$

where some of the symbols remain to be defined. $\mathbf{B}_0$ is a constant, uniform magnetic field in the z direction, $B_0\hat{\mathbf{e}}_z$, and accounts for all the toroidal flux $B_0\pi a^2$, since all the other functions are "fluxless." χ_{nmq} is a solution of Laplace's equation $\nabla^2\chi_{nmq}=0$, and is written

$$\chi_{nmq}=\begin{cases}ib_{nmq}I_m(k_n r)e^{i(m\varphi+k_n z)}, & n\neq 0\\ ib_{0mq}r^m e^{im\varphi}, & n=0 \text{ and } m\neq 0\\ 0, & n=0=m\ .\end{cases} \tag{5.3}$$

The real numbers b_{nmq} and b_{0mq} are determined by the boundary condition $\mathbf{B}\cdot\hat{\mathbf{n}}=0$ at $r=a$. The last term of (5.2) is a poloidal contribution whose curl leads to the average toroidal current contribution that follows from (4.10).

All terms in (5.2) are thus completely determined except the overall amplitude ζ_{nmq}. Since the ib_{nmq} will be proportional to the id_{nmq}, notice that every term in (5.2) *except* $\mathbf{B}_0$ contains a multiplicative factor of ζ_{nmq}. β_{00q} is responsible for all the toroidal current, and there is none for modes with $n^2+m^2>0$. $\mathbf{B}_0$ is responsible for the total toroidal flux, which is always $B_0\pi a^2$ regardless of m and n.

VI. SEARCH FOR THE MINIMUM-DISSIPATION STATE

The only undetermined number in $\mathbf{j}_{nmq}$ and $\mathbf{B}_{nmq}$ is now the overall amplitude ζ_{nmq}, given n, m, and q. The problem has been reduced to finding the minimum value of $\langle j_{nmq}^2\rangle$, subject to a given value of $K\equiv\langle \mathbf{j}_{nmq}\cdot\mathbf{B}_{nmq}\rangle$, with $\mathbf{j}_{nmq}$ and $\mathbf{B}_{nmq}$ given by (4.1) and (5.2). It is possible to prove a very useful relation between these volume averages, which we now demonstrate.

First, consider the case $n^2+m^2>0$. Substitute (4.1) into $\int \mathbf{j}_{nmq}\cdot\mathbf{B}_{nmq}d^3x$ to get (real parts understood *before* multiplication)

$$\int \mathbf{j}_{nmq}\cdot\mathbf{B}_{nmq}d^3x$$
$$=\int d^3x\left[\zeta_{nmq}\mathbf{J}_{nmq}+\frac{\nabla s_{nmq}}{\lambda_{nmq}}\right]\cdot\mathbf{B}_{nmq}\ . \tag{6.1}$$

The last term in (6.1) vanishes upon conversion to a surface integral and using the boundary conditions; for the rest, we may write

$$\int d^3x\,\zeta_{nmq}\mathbf{J}_{nmq}\cdot\mathbf{B}_{nmq}$$
$$=\int d^3x\frac{(\nabla\times\zeta_{nmq}\mathbf{J}_{nmq})}{\lambda_{nmq}}\cdot\mathbf{B}_{nmq}$$
$$=\int d^3x\frac{1}{\lambda_{nmq}}\nabla\times\left[\zeta_{nmq}\mathbf{J}_{nmq}+\frac{1}{\lambda_{nmq}}\nabla s_{nmq}\right]\cdot\mathbf{B}_{nmq}\ . \tag{6.2}$$

The larger parentheses in (6.2) is $\mathbf{j}_{nmq}$, so we have proved that

$$\int \mathbf{j}_{nmq}\cdot\mathbf{B}_{nmq}d^3x=\frac{1}{\lambda_{nmq}}\int d^3x\,(\nabla\times\mathbf{j}_{nmq})\cdot\mathbf{B}_{nmq}$$
$$=\frac{1}{\lambda_{nmq}}\int\nabla\cdot(\mathbf{j}_{nmq}\times\mathbf{B}_{nmq})d^3x$$
$$+\frac{1}{\lambda_{nmq}}\int\nabla\times\mathbf{B}_{nmq}\cdot\mathbf{j}_{nmq}d^3x$$
$$=\frac{1}{\lambda_{nmq}}\int d^3x\,j_{nmq}^2\ , \tag{6.3}$$

$$F=\frac{\zeta_{001}\gamma_{001}J_0(\gamma_{001}a)}{B_0}+1$$
$$=+1+\frac{J_0^2(\gamma_{001}a)[1-\sqrt{1+(2/\Pi_B)}]}{2\{2J_0^2(\gamma_{001}a)+[J_1'(\gamma_{001}a)]^2\}}$$
$$=1+\tfrac{1}{6}[1-\sqrt{1+(2/\Pi_B)}]\ . \qquad (6.19)$$

This follows from

$$\mathbf{B}_{001}(r)\cdot\hat{\mathbf{e}}_z/B_0$$
$$=1+(\tfrac{1}{6})[1-\sqrt{1+2/\Pi_B}]\cdot J_0(\gamma_{001}r)/J_0(\gamma_{001}a)\ ;$$

also

$$\Theta=\frac{(a\lambda_{001})J_0^2(\lambda_{001}a)}{4\{2J_0^2(\lambda_{001}a)+[J_1'(\lambda_{001}a)]^2\}}$$
$$\times[-1+\sqrt{1+(2/\Pi_B)}]$$
$$\cong 0.32[-1+\sqrt{1+(2/\Pi_B)}]\ . \qquad (6.20)$$

Combining these two expressions gives

$$F\cong 1-0.52\Theta\ . \qquad (6.21)$$

Field reversal occurs at $\Theta\cong 1.9$ (instead of 1.2, as in the "minimum-energy" formulation), and the minimum-energy-dissipation state ceases to be the 001 state at

$$\Theta\cong 0.32[-1+\sqrt{1+2/(0.022)}]\simeq 2.75$$

(instead of 1.6, as in the minimum-energy formulation).

The toroidal current density of the 001 state is

$$\mathbf{j}_{001}\cdot\hat{\mathbf{e}}_z=\zeta_{001}\gamma_{001}^2[J_0(\gamma_{001}r)-J_0(\gamma_{001}a)]\ , \qquad (6.22)$$

which remains always positive and goes smoothly to zero at $r=a$. The toroidal magnetic field is given by

$$\mathbf{B}_{001}\cdot\hat{\mathbf{e}}_z=\zeta_{001}\gamma_{001}J_0(\lambda_{001}r)+B_0\ . \qquad (6.23)$$

Equation (6.23) is the magnetic field of the "Taylor state" plus a a constant. Whether or not it reverses before $r=a$ depends upon Π_B (or Θ), as we have already seen. Up to an additive constant, (6.22) is also the toroidal current associated with the "Taylor state;" the constant is the constant necessary to bring $j_z(r)$ smoothly to zero at $r=a$.

Some typical profiles of the 001 minimum-dissipation state are illustrated in Figs. 1–5. Figures 1–5 refer to the case $B_0=0.5$, $a=\pi/2$, $\Pi_B=0.025$. This is a state close to the upper limit in Θ of the "window" in which the minimum-dissipation state is the field-reversed 001 state. Figures 1–5 are obtained by numerically evaluating Eqs. (6.9) and (6.10) for $q=1$, and plotting the evaluated quantities versus r.

Figure 1 is $B_z(r)$ as a function of r. Figure 2 is $j_z(r)$ as a function of r. Figure 3 is the radial component of $\mathbf{j}\times\mathbf{B}$ as a function of r, and is the only nonvanishing component of that vector. Note that the magnitude of $\mathbf{j}\times\mathbf{B}$ is much less than $|\mathbf{j}|\cdot|\mathbf{B}|$, indicating proximity to a force-free state. Figure 3 is a direct measure of the radial pressure gradient that the minimum-dissipation state will support. Figure 4 is a plot of the "alignment cosine" $\mathbf{j}\cdot\mathbf{B}/jB$, which measures the departure from the force-free condition. Note the presence of a force-free core surrounded by a region which is less so centered just above $r=1$. Finally, Fig. 5 is a plot of the ratio $\mathbf{j}\cdot\mathbf{B}/B^2$, which varies considerably more than the alignment cosine. Figures 4 and 5 are in qualitative agreement with the results of dynamical computations.

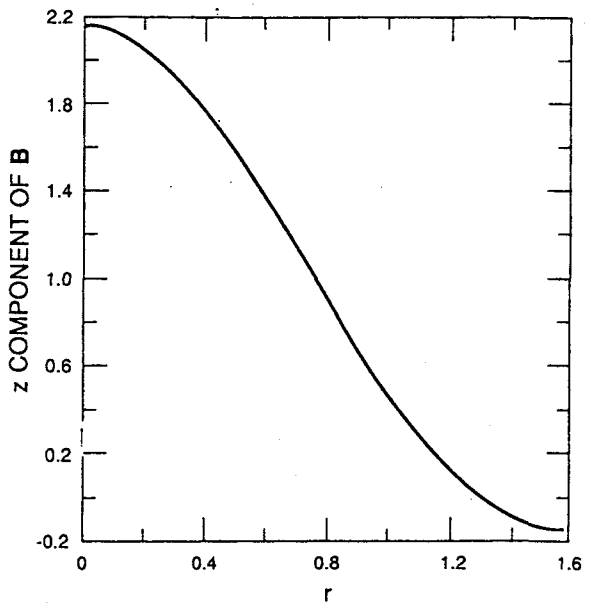

FIG. 1. $B_z(r)$ vs r, for the case $a=\pi/2$, $B_0=\frac{1}{2}$, $\Pi_B=0.025$ and $\Theta\cong 2.56$. [All graphs are in the dimensionless units of Eqs. (2.1)–(2.4).]

VII. SUMMARY

We have explored the consequences of the assumption that time-averaged magnetic profiles in a current-carrying conducting magnetofluid may be determined by minimizing the rate of energy dissipation. For the case of

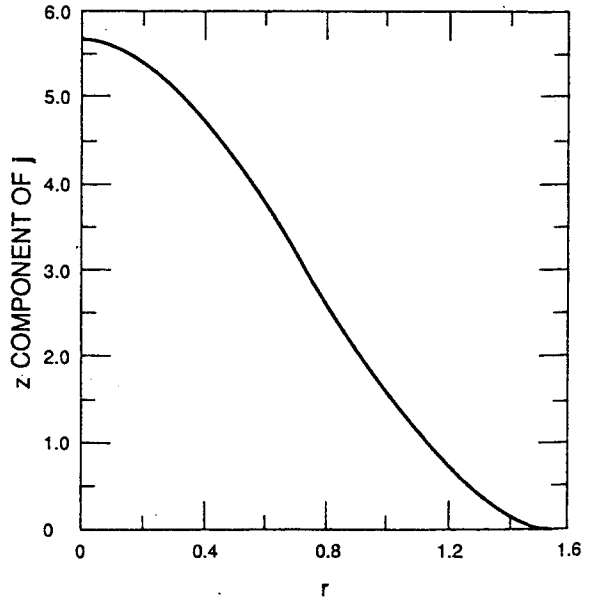

FIG. 2. $j_z(r)$ vs r, same case as Fig. 1.

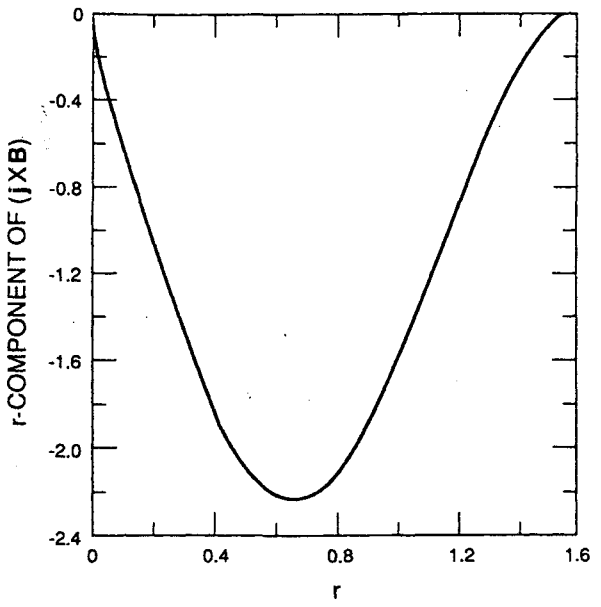

FIG. 3. $(\mathbf{j}\times\mathbf{B})_r$ vs r, same case as Fig. 1.

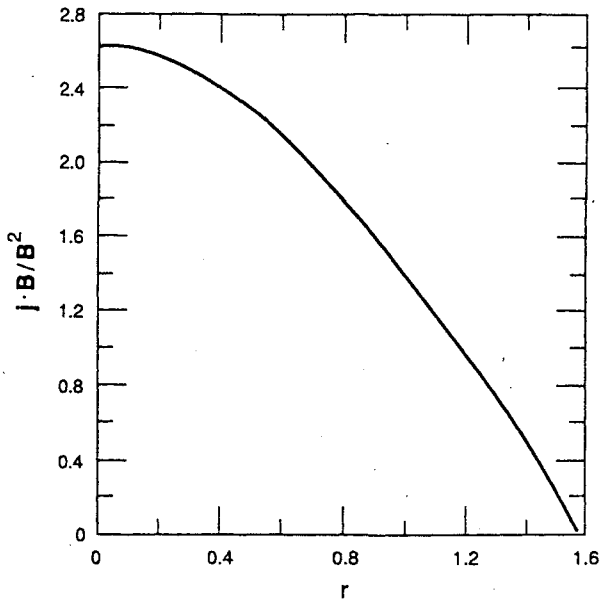

FIG. 5. Plot of $\Lambda\equiv\mathbf{j}\cdot\mathbf{B}/B^2$ vs r, same case as Fig. 1.

a uniform, incompressible magnetofluid with constant dissipation coefficients, to which these calculations are limited, this is equivalent to the principle of minimum entropy production, if the primitive definition of entropy is adopted.

The variational equation which results, for perfectly conducting boundaries with the current density unrestricted at the wall, or normal to the wall, is Eq. (3.3), with s a solution of Laplace's equation. The range of possible solutions to (3.3) is wide. For the case of the current unrestricted at the wall, the implications of the theory seem to be those of Taylor's "minimum-energy" theory. For the case in which the tangential component of the current vanishes at the wall, the results differ in several respects. It seems likely that any other possible boundary conditions will result in predictions which differ in other ways. One result that the current boundary conditions do yield is a finite value of $(\mathbf{j}\times\mathbf{B})\cdot\hat{\mathbf{e}}_r$, providing some confinement.

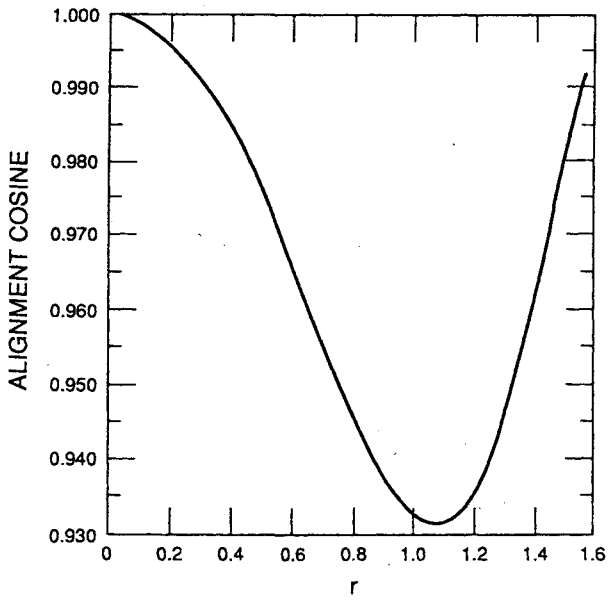

FIG. 4. Alignment cosine, $\mathbf{j}\cdot\mathbf{B}/jB$, same case as Fig. 1.

A time-averaged pressure, to go with each magnetic profile, may be inferred from Eq. (2.1). One takes the divergence *before* time averaging, and solves the resulting Poisson equation for p. If $\bar{\mathbf{j}}\times\bar{\mathbf{B}}\neq 0$, $\nabla\bar{p}$ will in general be nonzero. It is interesting that below the value of Θ for which field reversal occurs, $(\mathbf{j}\times\mathbf{B})\cdot\hat{\mathbf{e}}_r$ develops a positive "hook" below $r=a$, which is an expelling, rather than a confining, force.

The principle itself is in the not entirely satisfactory position of having been proved, but under less than general conditions, that do not fully cover the cases to which we wish to apply it. This issue has been worried about by others[23,24] in the hydrodynamic context, and we do not expect an easy or early resolution to it. For purposes of this paper, it stands only as a conjecture, though potentially a numerically testable one. (See also Jaynes.[25])

Notice that the principle as given does not demand that the profiles calculated be stable or even time stationary. All that is required is that the fluctuations about them be fractionally small. There is also no reliance upon inverse cascade processes, or their close relatives, "selective decay" and "dynamic alignment."

The axisymmetric state, 001 [Eqs. (6.9) and (6.10)], is predicted up to a value of the pinch parameter $\Theta\cong 2.75$, and the toroidal magnetic field [Eq. (6.23)] reverses above $\Theta\cong 1.9$, for the $\mathbf{j}\times\hat{\mathbf{n}}=\mathbf{0}$ boundary conditions. The resulting F-Θ diagram, $F\cong 1-0.52\Theta$, lies above points which have been observed in several experiments (cf. Taylor,[12] for example, Figs. 3, 5, and 6). The experimental points, however, consistently lie well above the F-Θ curve predicted by the minimum-energy principle, whose "window" of axisymmetric reversed-field operation lies[9-12] between $\Theta\simeq 1.2$ and 1.6. It seems likely that the region between the two curves is accessible to more exotic boundary conditions. The toroidal current [Eq. (6.22)]

$$\frac{\partial \underset{\sim}{v}}{\partial t} + \underset{\sim}{v} \cdot \nabla \underset{\sim}{v} = -\nabla(p/\rho) + \underset{\sim}{j}/c \times \underset{\sim}{B} + \nu \nabla^2 \underset{\sim}{v}$$

$$\nabla \cdot \underset{\sim}{v} = 0, \quad \rho = \text{const.}$$

$$\nabla \times \underset{\sim}{B} = \frac{4\pi}{c} \underset{\sim}{j}$$

$$\nabla \cdot \underset{\sim}{B} = 0$$

$$\frac{\partial \underset{\sim}{B}}{\partial t} = -c \nabla \times \underset{\sim}{E}$$

$$\underset{\sim}{E} + \underset{\sim}{v}/c \times \underset{\sim}{B} = \underset{\sim}{j}/\sigma$$

In steady state, $\frac{\partial}{\partial t} = 0$, $\underset{\sim}{E} = -\nabla \Phi$

If $\underset{\sim}{v} = 0$,

$$\nabla \cdot \underset{\sim}{j} = 0 = \nabla \cdot (\sigma \nabla \Phi)$$

If $\sigma = \text{const.}$, $\nabla^2 \Phi = 0$

Giving Φ over boundary (or $\hat{n} \cdot \nabla \Phi$)

will determine $\Phi \Rightarrow \underset{\sim}{E} \Rightarrow \underset{\sim}{j} \Rightarrow \underset{\sim}{B}$

$\nabla \times \underset{\sim}{j} = 0$, then, for any steady state.

Any variation in profile appears to originate in spatial dependence of σ: $\sigma = \sigma(\underset{\sim}{x})$.

Calculating $\sigma(\underset{\sim}{x})$ self-consistently would involve adding an energy equation to the description (prohibitive).

Simplest steady state: cylindrical geometry.

$$\underset{\sim}{E} = E_0 \hat{e}_z$$

$$\underset{\sim}{j} = j_0 \hat{e}_z = \sigma \underset{\sim}{E}, \quad \sigma = \text{const.}$$

$$\underset{\sim}{B} = B_0 \hat{e}_z + \frac{2\pi j_0}{cr} \hat{e}_\varphi r^2$$

$$= B_0 \hat{e}_z + \frac{2\pi j_0 r}{c} \hat{e}_\varphi$$

$$p = \frac{\pi j_0^2}{c^2}(a^2 - r^2)$$

$$\underset{\sim}{v} = 0$$

Try $\underset{\sim}{B} = \underset{\sim}{B}^{(0)} + \epsilon \underset{\sim}{B}^{(1)} + \epsilon^2 \underset{\sim}{B}^{(2)} + \cdots$

$\underset{\sim}{j} = j_0 \hat{e}_z + \epsilon \underset{\sim}{j}^{(1)} + \epsilon^2 \underset{\sim}{j}^{(2)} + \cdots$

$\underset{\sim}{v} = \epsilon \underset{\sim}{v}^{(1)} + \epsilon^2 \underset{\sim}{v}^{(2)} + \cdots$

$\underset{\sim}{\omega} = \epsilon \underset{\sim}{\omega}^{(1)} + \epsilon^2 \underset{\sim}{\omega}^{(2)} + \cdots$

$$\begin{pmatrix} \underset{\sim}{B}^{(1)} \\ \underset{\sim}{j}^{(1)} \\ \underset{\sim}{v}^{(1)} \\ \underset{\sim}{\omega}^{(1)} \end{pmatrix} \sim e^{-i\omega t + ikz}$$

$\underset{\sim}{v}^{(1)} \cdot \hat{n} = \underset{\sim}{\omega}^{(1)} \cdot \hat{n} = 0$

$\underset{\sim}{B}^{(1)} \cdot \hat{n} = \underset{\sim}{j}^{(1)} \cdot \hat{n} = 0$

periodic in z

STABILITY BOUNDARY IS EXACTLY SOLUBLE

Eigenfunctions are Chandrasekhar - Kendall functions,

$$\nabla \times \underset{\sim}{A} = \lambda \underset{\sim}{A} \quad , \quad \lambda^2 = \gamma^2 + k^2 ,$$

$$\underset{\sim}{A} = C\left[\nabla \times (\nabla \times \hat{e}_z \varphi) + \frac{1}{\lambda} (\nabla \times \hat{e}_z \varphi) \right]$$

$$(\nabla^2 + \lambda^2)\, \varphi = 0$$

$$\varphi = \exp\left[-i\omega t + ikz + im\varphi\right] J_m(\gamma r)$$

For given aspect ratio, L_z/a, stability boundary is a curve in the Θ, H plane.

Θ = pinch ratio = $\dfrac{B_\theta(a)}{B_0}$

H = Hartmann number = $\dfrac{C_A\, a}{\sqrt{\nu\eta}}$

$C_A = B_0/\sqrt{4\pi\rho}$ = Alfvén speed

$\eta = c^2/4\pi\sigma$ = magnetic diffusivity

General shape:

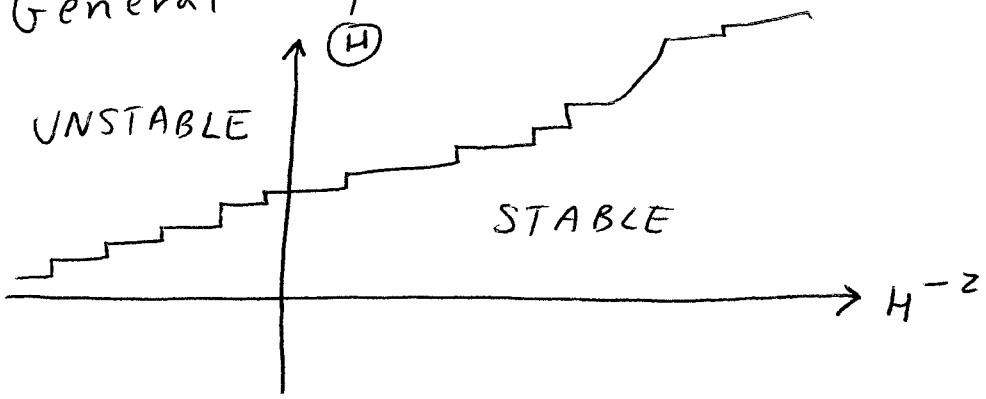

Slightly above stability threshold,

A STEADY STATE CAN BE CONSTRUCTED

THROUGH FIRST THREE ORDERS IN

PERTURBATION THEORY; IT IS HELICAL

AND INVOLVES FLOW.

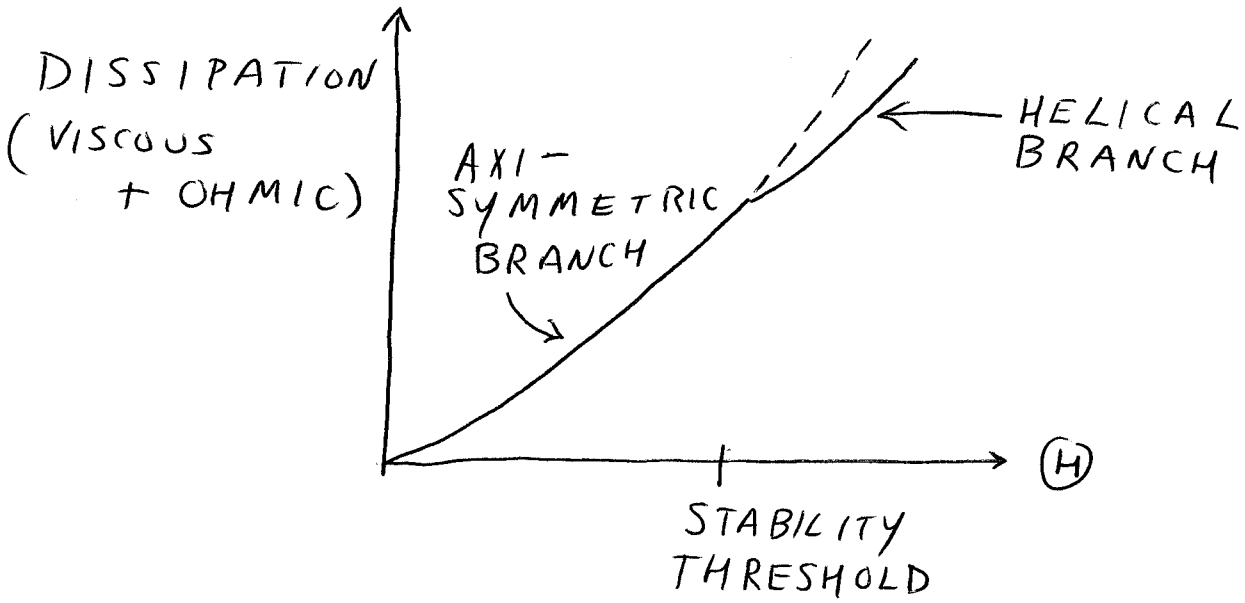

X. SHAN et al,

Phys. Rev. A 44, 6800 (1991).

Plasma Phys. & Contr. Fusion 35,
619 and 1019 (1993).

Phys. Rev. Lett. 73, 1624 (1994).

$$\mathbf{v}^{(1)}=\frac{\eta\lambda^2}{(mj_0/2)-k_nB_0}$$
$$\times(A\cos\psi\hat{\mathbf{e}}_r+B\sin\psi\hat{\mathbf{e}}_\varphi+C\sin\psi\hat{\mathbf{e}}_z)\ . \tag{21}$$

Also, $\mathbf{j}^{(1)}=\lambda\mathbf{B}^{(1)}$ and $\omega^{(1)}=\lambda\mathbf{v}^{(1)}$.

The inhomogeneous terms which generate the second-order solution are

$$\mathbf{v}^{(1)}\times\omega^{(1)}=0\ , \tag{22a}$$

$$\mathbf{j}^{(1)}\times\mathbf{B}^{(1)}=0\ , \tag{22b}$$

and

$$\mathbf{v}^{(1)}\times\mathbf{B}^{(1)}=\frac{\eta\lambda^2}{(mj_0/2)-k_nB_0}(-AC\hat{\mathbf{e}}_\varphi+AB\hat{\mathbf{e}}_z)\ . \tag{22c}$$

The fact that $\mathbf{v}^{(1)}\times\mathbf{B}^{(1)}$ is a function of r only and has only $\hat{\mathbf{e}}_\varphi$ and $\hat{\mathbf{e}}_z$ components is what makes the solution possible in second order. For now, inserting Eqs. (22) into Eqs. (9) and (10), we see that it is possible to find the second-order solution as essentially a correction to the zeroth order,

$$\mathbf{v}^{(2)}=0\ , \tag{23a}$$

$$\mathbf{j}^{(2)}=\frac{1}{\eta}\mathbf{v}^{(1)}\times\mathbf{B}^{(1)}$$
$$=\frac{1}{\eta}\left[\frac{\eta\lambda^2}{(mj_0/2)-k_nB_0}\right](-AC\hat{\mathbf{e}}_\varphi+AB\hat{\mathbf{e}}_z)\ , \tag{23b}$$

with the easy equation

$$\nabla\times\mathbf{B}^{(2)}=\mathbf{j}^{(2)} \tag{23c}$$

to be solved for $\mathbf{B}^{(2)}$. Note that $\mathbf{j}^{(1)}\cdot\hat{\mathbf{n}}=0=\mathbf{j}^{(2)}\cdot\hat{\mathbf{n}}$ at $r=a$, compatible with the insulating layer's presence there. The fields $\mathbf{v}^{(2)}$, $\mathbf{B}^{(2)}$ will also obey all the boundary conditions. $\mathbf{B}^{(2)}$ will be an axisymmetric function of r with only $\hat{\mathbf{e}}_\varphi$ and $\hat{\mathbf{e}}_z$ components. A constant must be added to $B_z^{(2)}$ to guarantee zero second-order toroidal flux.

We now have the solution through the first two orders beyond the axisymmetric state. Of course, the zeroth-order solution, without any $\mathbf{v}^{(1)}$, $\mathbf{B}^{(1)}$, etc., is still a solution also, for the same parameters. It is known to be the minimum dissipation state for this problem,[2,3] with $\mathbf{v}=0$ by assumption, for low enough E_{ext}, providing that the same boundary conditions are employed. We must now compare the dissipation rates for the two states.

III. THE DISSIPATION RATES

The total dissipation rate before any expansions are performed is

$$R\equiv\eta\langle\mathbf{j}^2\rangle+\nu\langle\omega^2\rangle\ . \tag{24}$$

For the axisymmetric $\mathbf{v}=0$ state, R is just $\eta j_0^2=E_{\text{ext}}^2/\eta$. The bracket $\langle\ \rangle$ will always mean a volume average.

Accurate through terms of second order, R becomes, in terms of the expansion of Eq. (5) and (6),

$$R=\eta\langle(\mathbf{j}^{(0)})^2\rangle+2\eta\langle\mathbf{j}^{(0)}\cdot\mathbf{j}^{(2)}\rangle$$
$$+\eta\langle(\mathbf{j}^{(1)})^2\rangle+\nu\langle(\omega^{(1)})^2\rangle+\cdots\ , \tag{25}$$

since $\langle\mathbf{j}^{(0)}\cdot\mathbf{j}^{(1)}\rangle=0$. The last two terms in Eq. (25) are positive definite, and the question is whether $2\eta\langle\mathbf{j}^{(0)}\cdot\mathbf{j}^{(2)}\rangle$ can be negative enough to pull the sum of the last three terms negative. We may consider the ratio

$$\mathcal{R}\equiv\frac{\eta\langle(\mathbf{j}^{(1)})^2\rangle}{2\eta\langle\mathbf{j}^{(0)}\cdot\mathbf{j}^{(2)}\rangle}+\frac{\nu\langle(\omega^{(1)})^2\rangle}{2\eta\langle\mathbf{j}^{(0)}\cdot\mathbf{j}^{(2)}\rangle}\equiv\mathcal{R}_1+\mathcal{R}_2\ . \tag{26}$$

If $\mathcal{R}$ is negative and lies between 0 and -1, the nonaxisymmetric state will have a lower dissipation rate than the axisymmetric one.

Since $\mathbf{j}^{(1)}=\lambda\mathbf{B}^{(1)}$ and $\omega^{(1)}=\lambda\mathbf{v}^{(1)}$, all the quantities in Eq. (26) can be calculated using Eqs. (20), (21), and (23b). The dispersion relation (16) at $\Omega=0$ can be used to simplify the result. After some algebra, we get

$$\mathcal{R}=-\frac{k_n}{4\lambda}\frac{\langle A^2+B^2+C^2\rangle}{\langle AB\rangle}\ , \tag{27}$$

where A, B, and C are defined between Eqs. (20) and (21). Using some obvious properties of the Chandrasekhar-Kendall functions, it can be straightforwardly shown that $\langle AB\rangle=(k_n/2\lambda)\langle A^2+B^2+C^2\rangle$, so that

$$\mathcal{R}=-\tfrac{1}{2}\ . \tag{28}$$

The simple result of Eq. (28) may be considered the principal result of this paper, since it demonstrates that, under the conditions assumed, the partially helical state with flow has a lower dissipation rate than the corresponding axisymmetric one, any time the stability threshold is reached.

We close this section by displaying some computer-drawn graphics which compare the nonaxisymmetric state calculated analytically in Sec. II with the results of previous dynamical computations[10] of solutions to the driven MHD equations in the Strauss approximation. Even though several details differ in the two situations, we believe the similarities to be somewhat striking. Comparison is made with the Strauss-approximation computations rather than the full three-dimensional (3D) MHD ones,[7–9] because, in the latter ones, emphasis was on the RFP state. It would not be expected that the perturbation theory could be pushed to high enough amplitudes to apprehend field reversal.

Figures 1 are two computer-drawn, three-dimensional, perspective plots of a surface of constant j_z. Figure 1(a) is obtained from the analytical function $\mathbf{j}^{(0)}+\mathbf{j}^{(1)}+\mathbf{j}^{(2)}$ given in this paper, and has the following dimensionless associated parameters: $L_z=4\pi$, $a=\pi/2$, $B_0=4.8$, $j_0=5.2$, $n=1$, $m=1$, and $\gamma a\cong4.45$. The displayed surface is $j_z=5.5$. The overall multiplicative amplitude, by which the helical magnetic field functions are multiplied before being added to the axisymmetric zeroth-order state, is 0.033. These parameters were chosen to match as closely as possible those of Fig. 1(b), which comes from

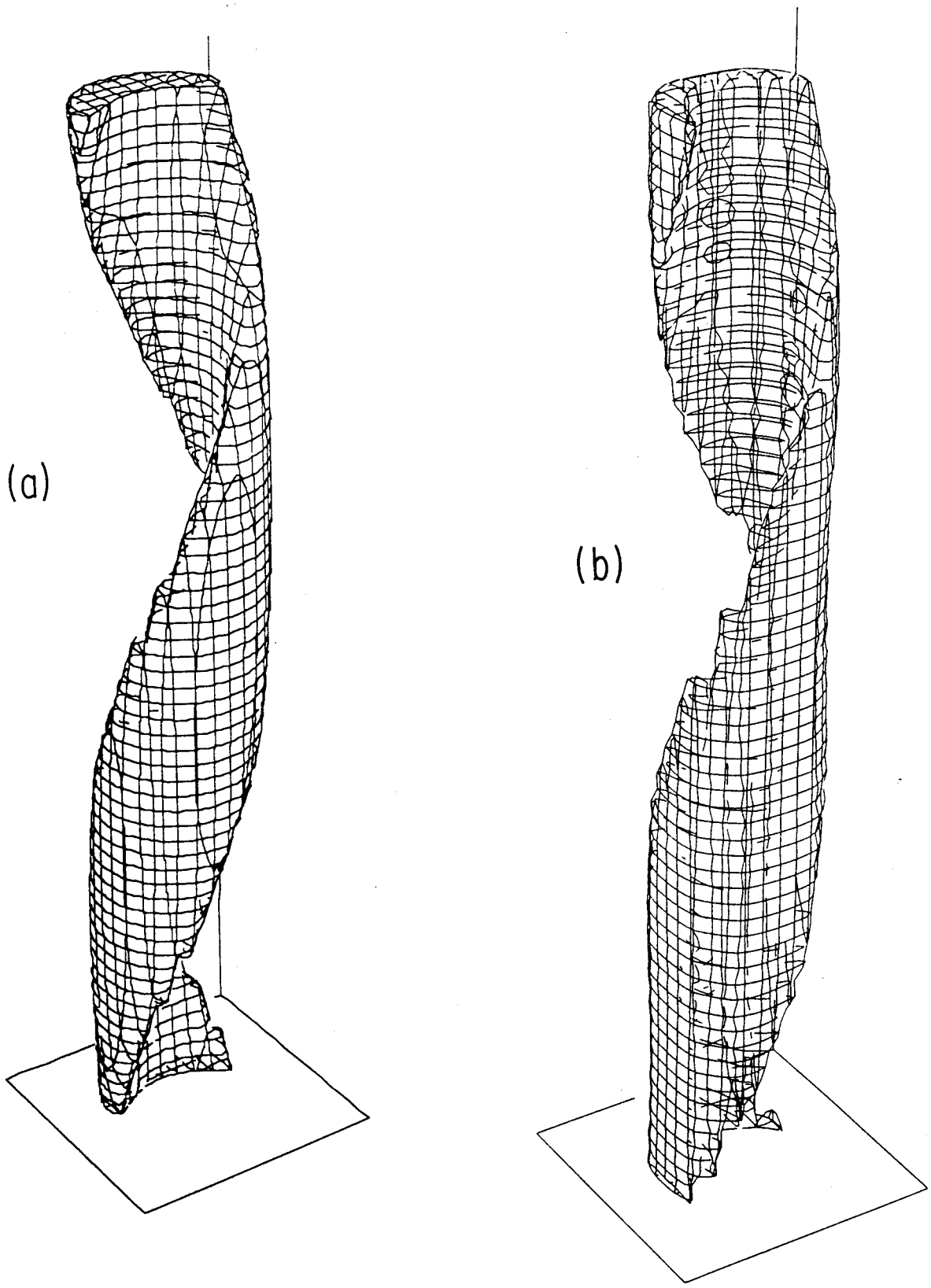

FIG. 1. Three-dimensional perspective plot of a $j_z = \text{const}$ surface, showing the helically kinked current channel: (a) the analytical solution from this paper; (b) an instantaneous snapshot of the numerical solution of the Strauss equations reported in Ref. 10. The circular-boundary analytical solutions are compared with the square-boundary computational ones by letting the circle be the largest one that can be inscribed in the square of edge π. Outside the radius $r = \pi/2$, the circular boundary solution has no physical meaning.

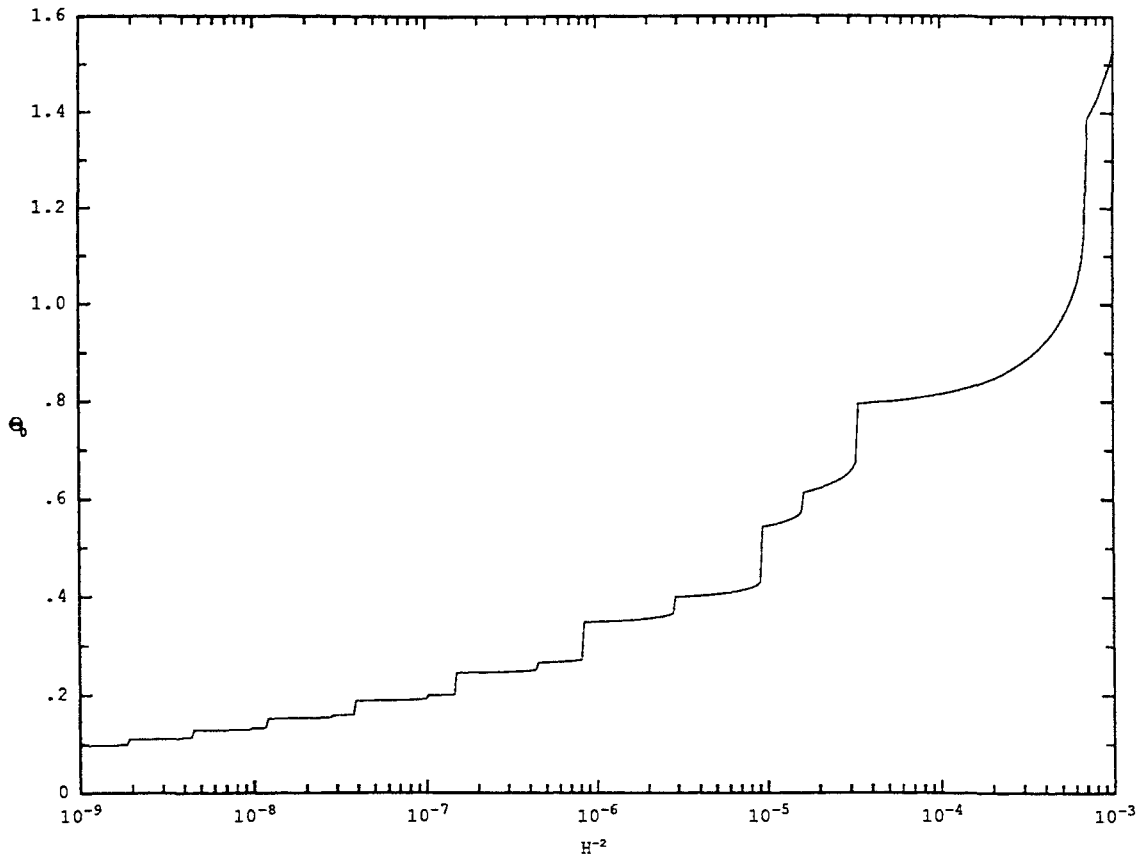

Figure 1.1: Threshold curve above which the zero-flow, uniform current profile is unstable. Axisymmetric zero-flow pinch ratio Θ_0 is plotted versus inverse Hartmann number squared. H^{-2} decreases linearly with decreasing $\eta\nu$ and Θ_0 increases with increasing toroidal voltage.

Notice the simple relation between the *pinch ratio* Θ_0 and the *safety factor* at the edge q_a in the axisymmetric, zero-flow state,

$$\Theta_0 = \frac{B_\varphi(a)}{B_0} = \alpha/q_a, \tag{1.23}$$

at the lowest order, namely $H \to \infty$, the threshold given by Eq. (1.20) can be equivalently expressed in terms of q_a, the safety factor at the wall, as

$$q_a > \frac{m}{n} + \frac{2}{\alpha\lambda a}, \tag{1.24}$$

which at the large aspect ratio ($\alpha \gg 1$) limit, is reduced to $q_a > m/n$. This is not to

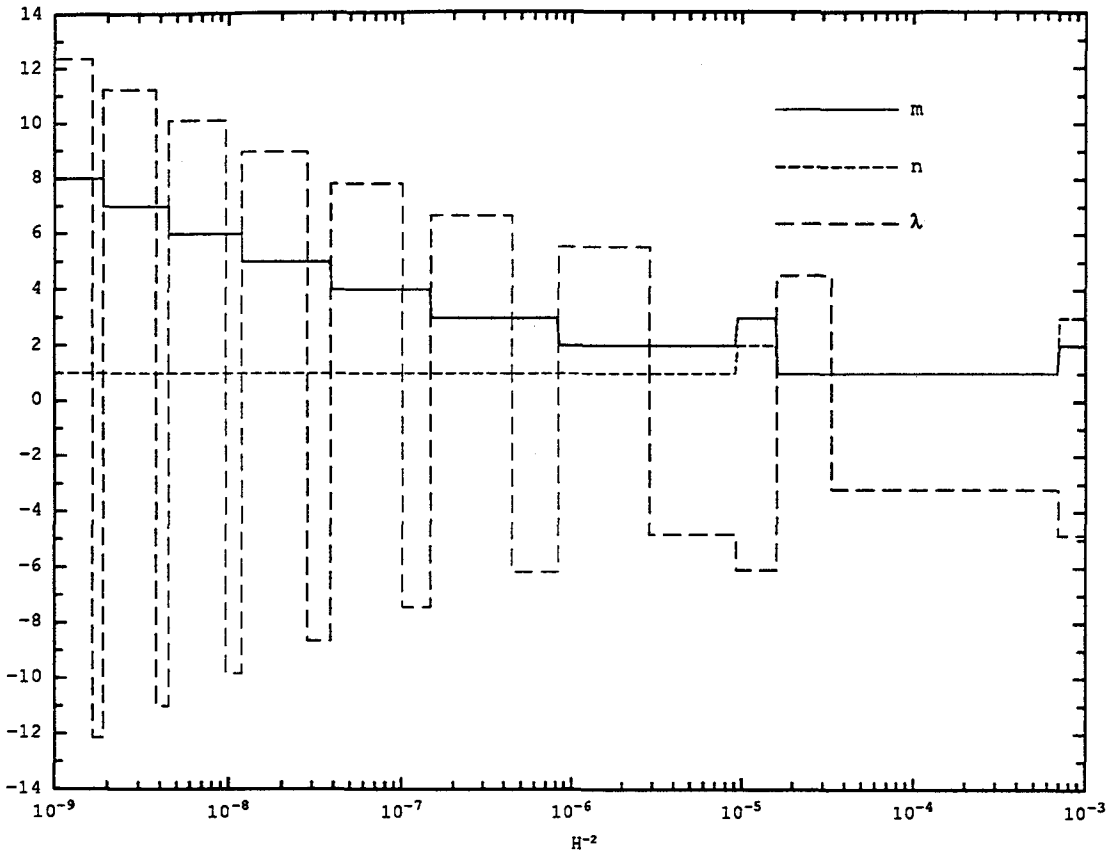

Figure 1.2: m, n and λ value of the first unstable mode as Θ_0 is raised above the threshold shown in Fig. 1.1. Shown as functions of H^{-2} for the inverse aspect ratio $\alpha^{-1} = \pi/4$.

which at the large aspect ratio ($\alpha \gg 1$) limit, is reduced to $q_a > m/n$. This is not to be considered as the same as the formally similar ideal stability condition derived for each kink mode with mode numbers m and n. In Eq. (1.24), m and n are to be read off Fig. 1.2 for given Hartmann numbers and are predicted as the mode numbers of the first unstable mode when q_a is lowered, or equivalently, when Θ_0 is raised.

The predictions of the principle of *minimum energy dissipation rate* are consistent with the repeated appearance of the partially-helical states with vortical flow in several fully three-dimensional computations [74, 75, 88–90] and are not inconsistent with the data from some confinement experiments. Further exploration of these minimum energy dissipation rate states will be one of the major tasks of this thesis.

equally among all the helical modes ($\mathbf{A}_{nmq}$ with $m^2 + n^2 \neq 0$). For the computation shown in Fig. 3.1 and Fig. 3.2, there are 330 independent modes present, including all those with $\lambda^2_{nmq} < 100$ for m and n not both zero. The $00q$ modes, up to $q = 10$, are required for the development of the radial variation in the current and magnetic field.

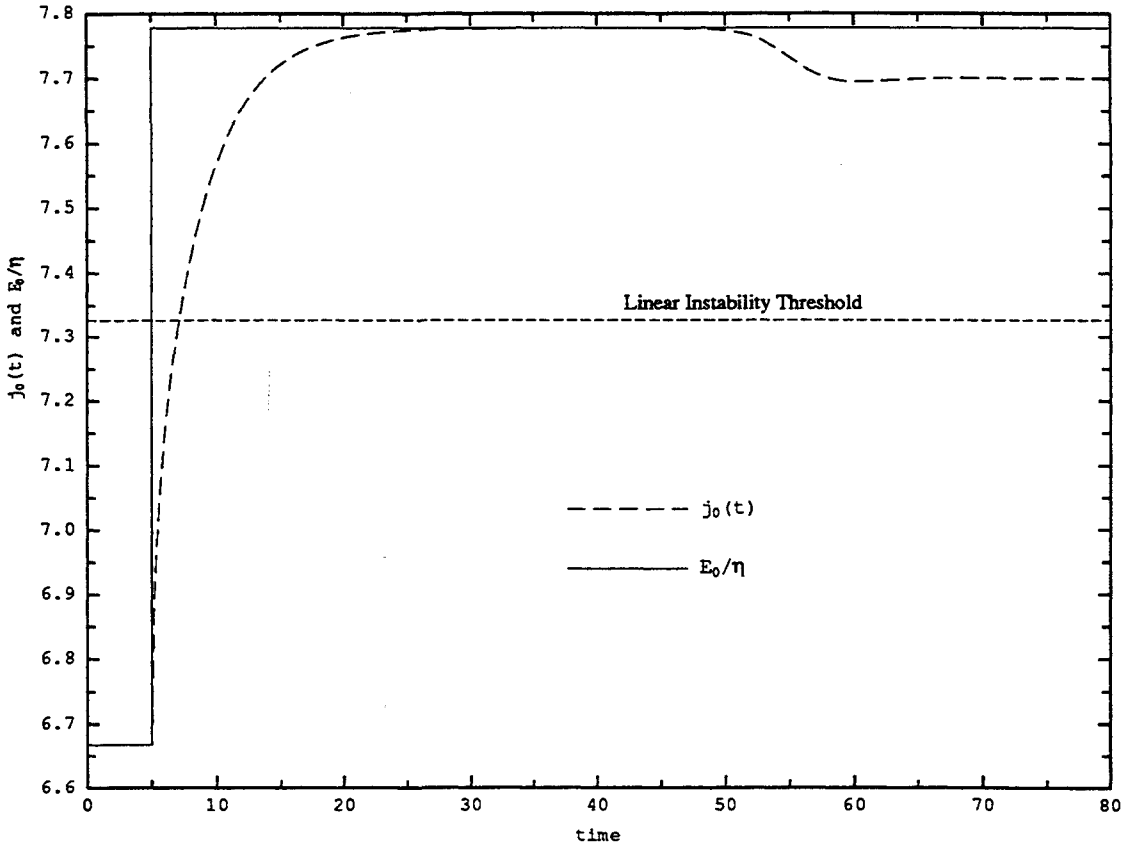

Figure 3.1: Time history of averaged current density j_0 and applied electric field divided by resistivity E_0/η, which is what the current density would be in an axisymmetric solution, plotted vs. t in poloidal Alfvén transit times. For this step in the electric field, the current crosses, between $t = 5$ and $t = 10$, the threshold for the appearance of the first linearly unstable mode. The dashed horizontal line is the current stability threshold.

The dashed curve in Fig. 3.1 is the axial current $j_0(t)$, which is following E_0/η, and by about $t = 20$ (times are always in poloidal Alfvén transit times), $j_0(t)$ has adjusted itself to the value $E_0/\eta \simeq 7.78$. Shown in Fig. 3.2 are the time histories of the kinetic,

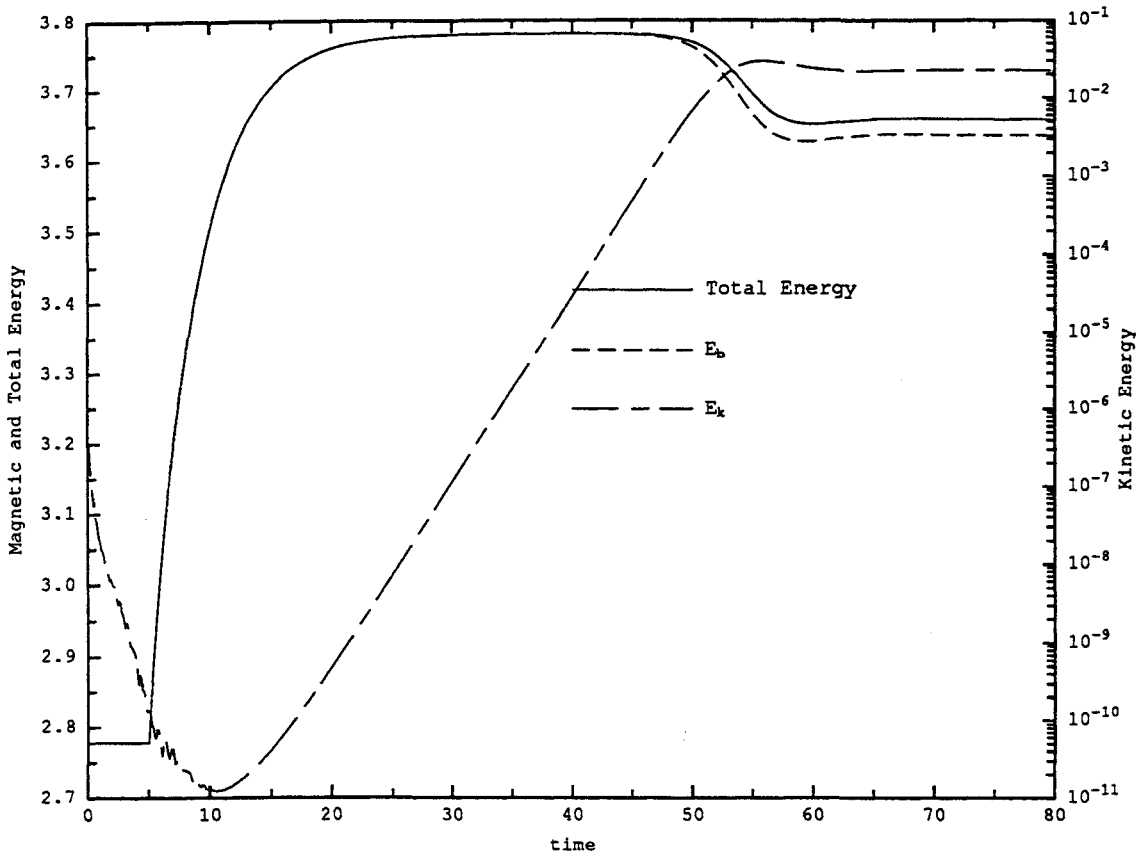

Figure 3.2: Time history of kinetic, magnetic and total energy for the same situation as shown in Fig. 3.1.

magnetic and total energy for the same situation. The total kinetic energy (the scale is on the right of the graph) is decaying from the initial random noise in the earliest stage when the current density is below the linear threshold.

As the current density j_0 approaches its new uniform value above the threshold just before $t = 20$, the kinetic energy begins to grow exponentially at a constant rate numerically measured to be 0.555, compared with a theoretical value of 0.558 [81]; this is thought to be satisfactory agreement. E_0 is held at this constant (supercritical) value and the kinetic energy ceases to grow at about $t = 50$. By $t = 60$, it has approached a constant value and there has been an accompanying depression of $j_0(t)$ to a constant value below E_0/η, (the global plasma resistivity increased). The magnetic energy also de-

creases a little because of this depression of the current density. It can be seen that after j_0 passes the linear threshold, the system undergoes a transition from the axisymmetric, uniform-current-density, no-flow, steady state to another steady state which is helically deformed and has finite amount of large scale vortical fluid motion. After $t = 60$, all quantities become time-independent and this saturated state with flow will apparently persist indefinitely.

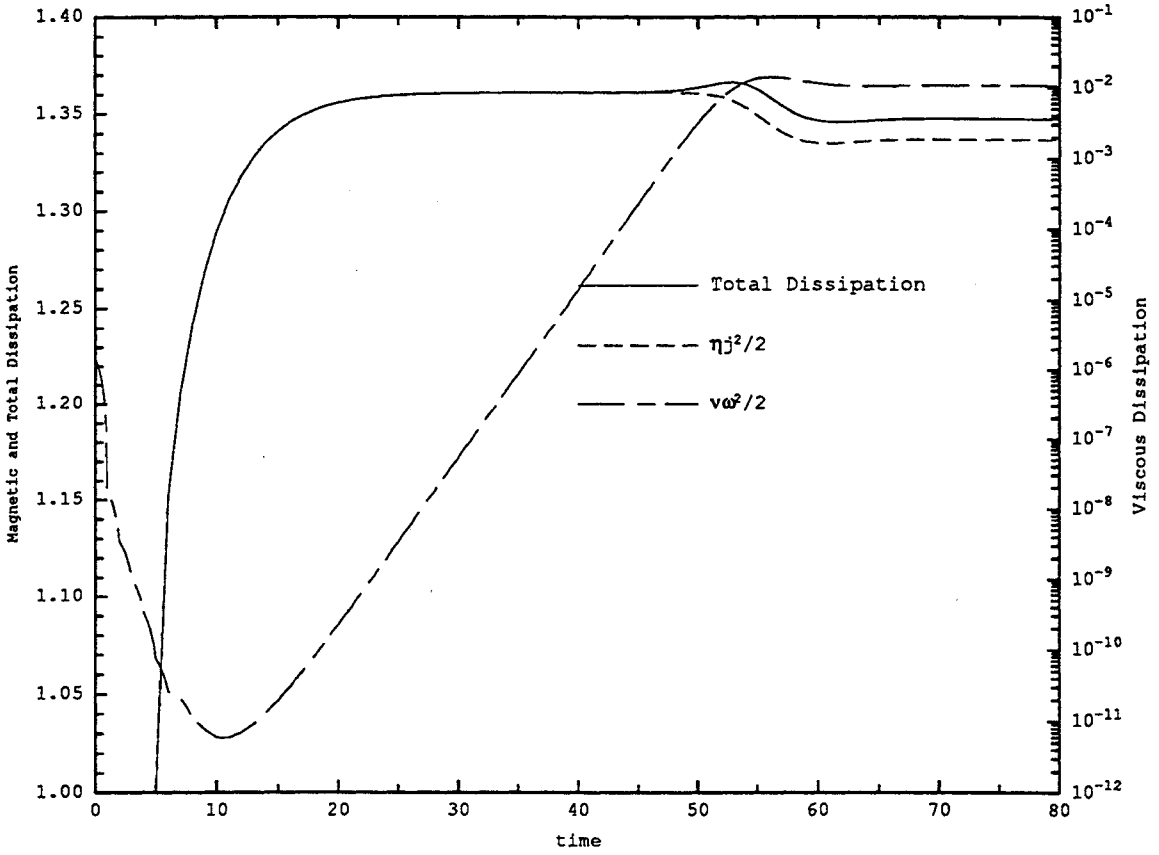

Figure 3.3: Time histories of the ohmic, viscous and total energy dissipation rates when the system undergoes a transition from the axisymmetric state to the helically deformed state. Note the *decrease* in the total energy dissipation rate after the transition.

Shown in Figure 3.3 are the ohmic, viscous and total energy dissipation rates as functions of time. It will be seen that the helical state the system bifurcated into has a lower total energy dissipation rate.

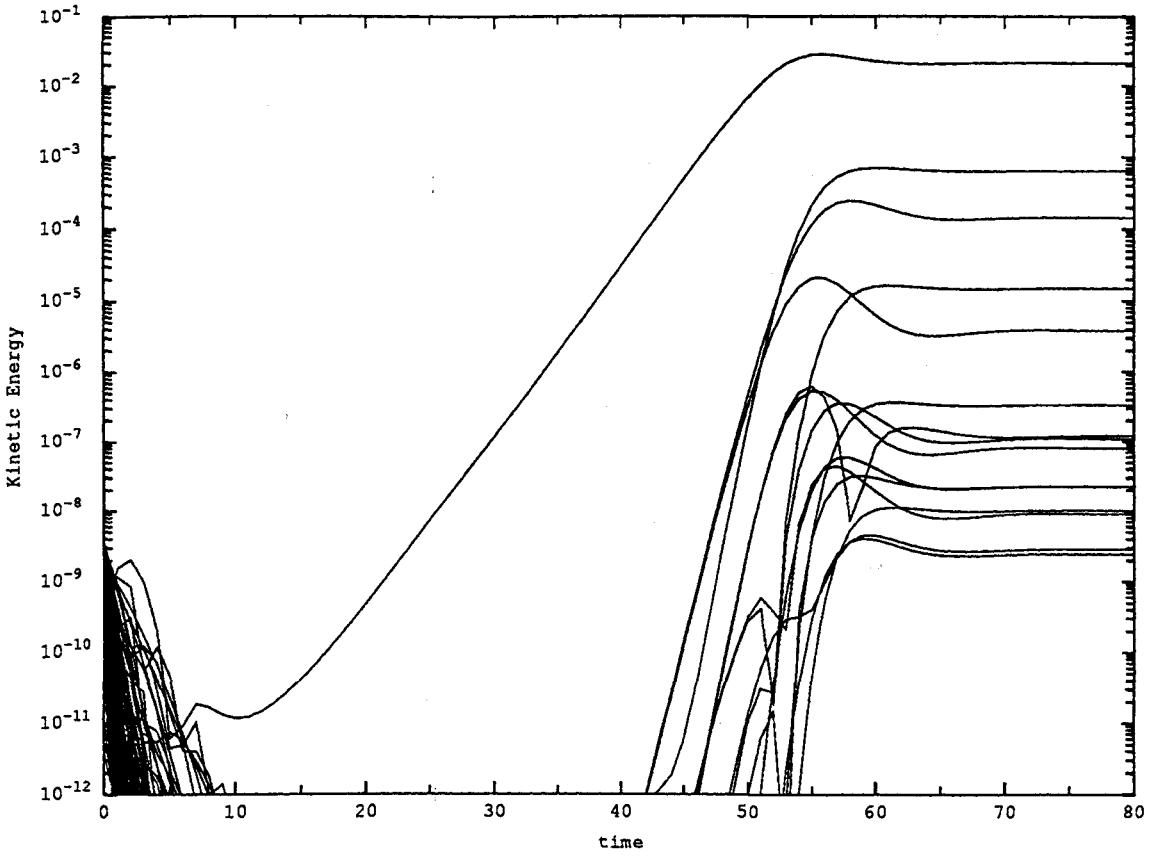

Figure 3.4: Time histories of the kinetic energies of the most energetic helical modes for the same situation as shown in Fig. 3.1. At $t = 0$, 320 helical modes are present. Note that a time-independent laminar state, where only a small number of modes are present, has been achieved by about $t = 65$. The dominant mode has $(m, n) = (1, 1)$, and second most dominant mode, down by over an order of magnitude, has $(m, n) = (2, 2)$.

Figures 3.4 and 3.5 show the time histories of the largest non-axisymmetric (i.e., those with m and n not both zero) modal kinetic and magnetic energies respectively. In the earliest subcritical stage, the majority of the modes simply damp away from the initial small random noise in about ten Alfvén times. At about $t \simeq 10$ when the averaged current density j_0 is raised above the linear instability threshold (cf. Fig. 3.1), as predicted by the linear theory, one single mode, identified as the first unstable mode (1,1,1), starts to grow exponentially at a constant rate. In the period between $t = 10$ and $t = 40$, when the departure from the uniform current density, zero flow equilibrium is small, the

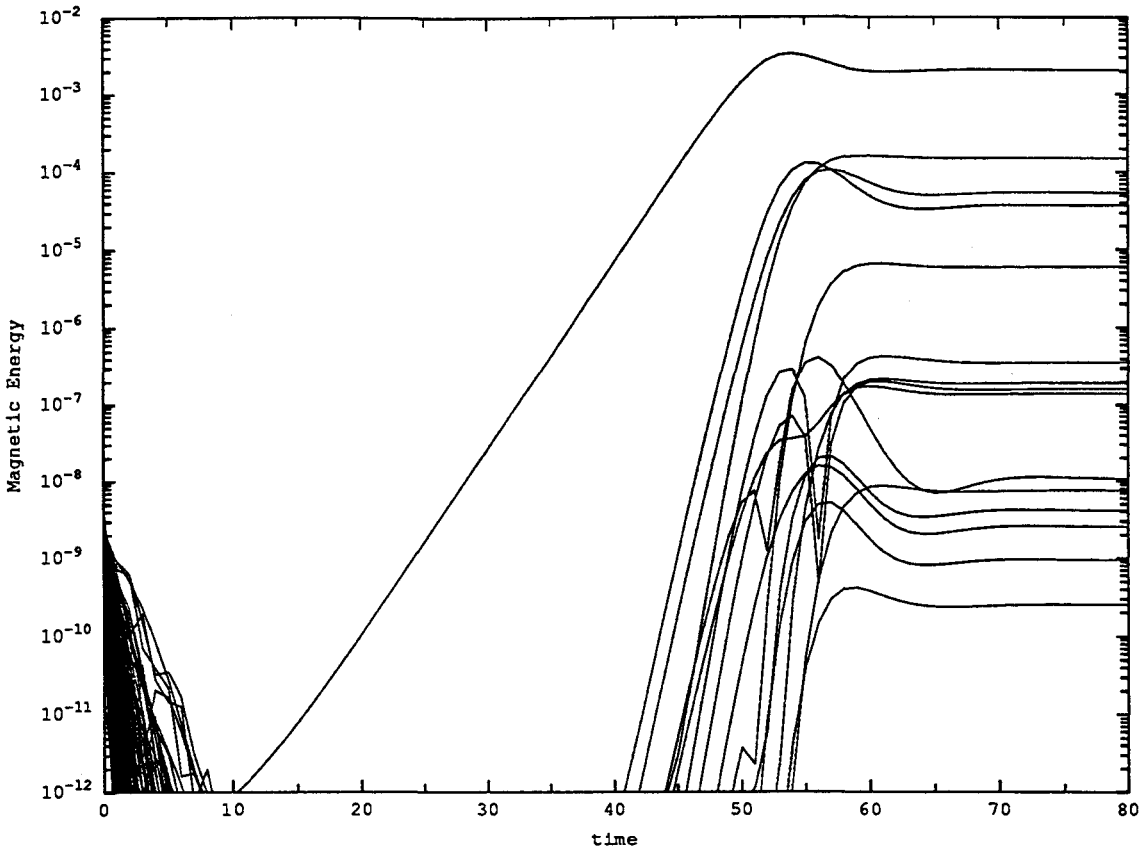

Figure 3.5: Time histories of the magnetic energies of the energetically largest helical modes for the same situation as shown in Fig. 3.4.

system is approximately axisymmetric and the linear theory is valid. At $t \simeq 40$, when the amplitude of the largest helical mode becomes so high that the linear theory ceases to apply, some other modes, identified either as (1,1) modes with higher radial mode number or the higher harmonics of the (1,1) mode, begin to participate and form a final helical equilibrium at $t > 60$.

Since the plot is logarithmic, it will be seen that for all practical purposes, the helical part of the final state is characterized by only a single Chandrasekhar-Kendall function and it is the $\mathbf{A}_{111}$ mode ($m = 1$, $n = 1$, $q = 1$). The second largest mode is smaller than the dominant mode by more than an order of magnitude. The single-mode, perturbation-theoretic, helical equilibrium [80], which consists only the $\mathbf{A}_{111}$ helical mode, appears to

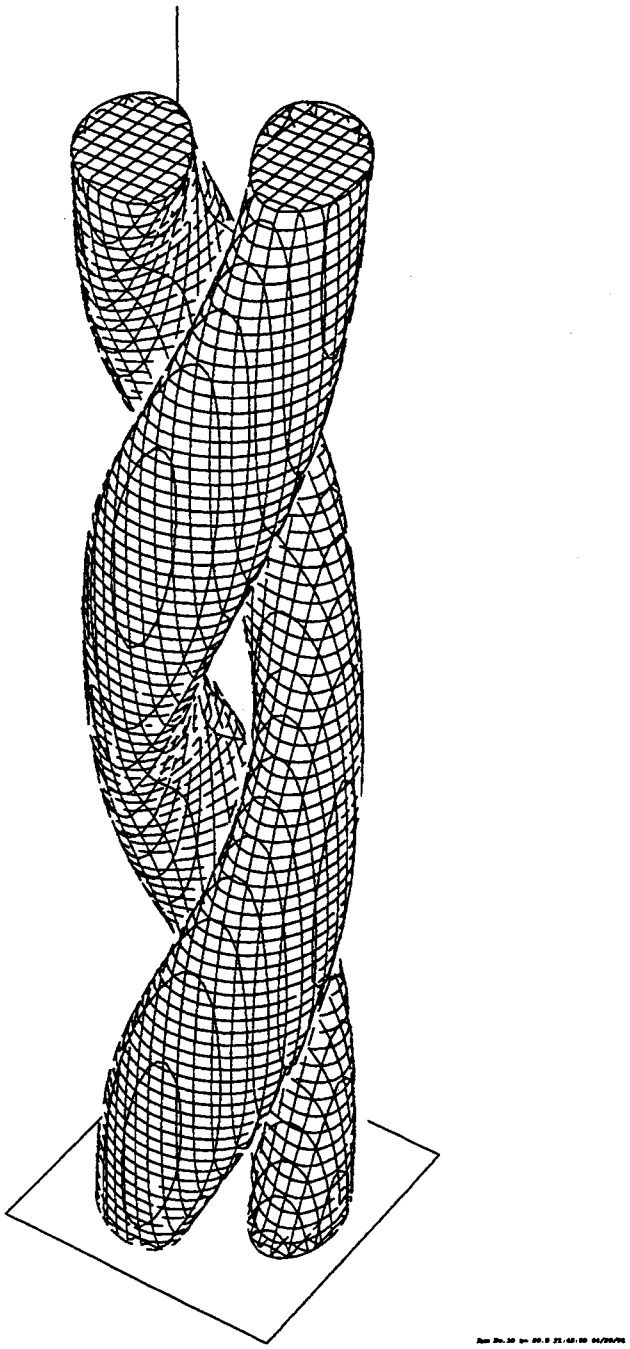

Figure 3.12: The three-dimensional perspective plot of a pair of the mass "flux surfaces." At any point on these surfaces the velocity field is tangent to the surface. Each of these surfaces defines a closed "flux tube." Axial cross sections of these surfaces are shown in Fig. 3.16.

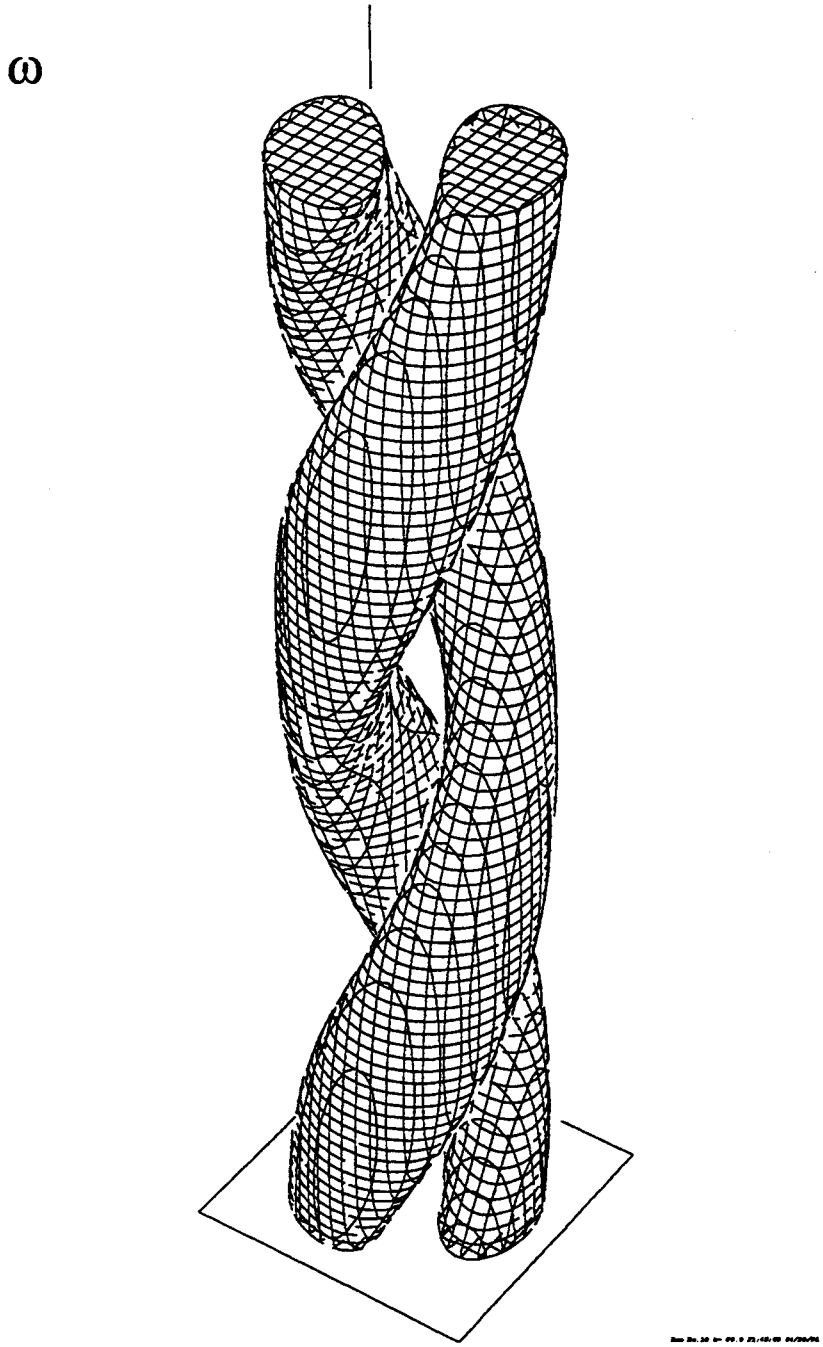

Figure 3.14: The three-dimensional perspective plot of a pair of the "vortex tubes," at any point on which, vorticity is tangent to the surface and the surface can be considered to be composed of "vorticity lines." Axial cross sections of these surfaces are shown in Fig. 3.18.

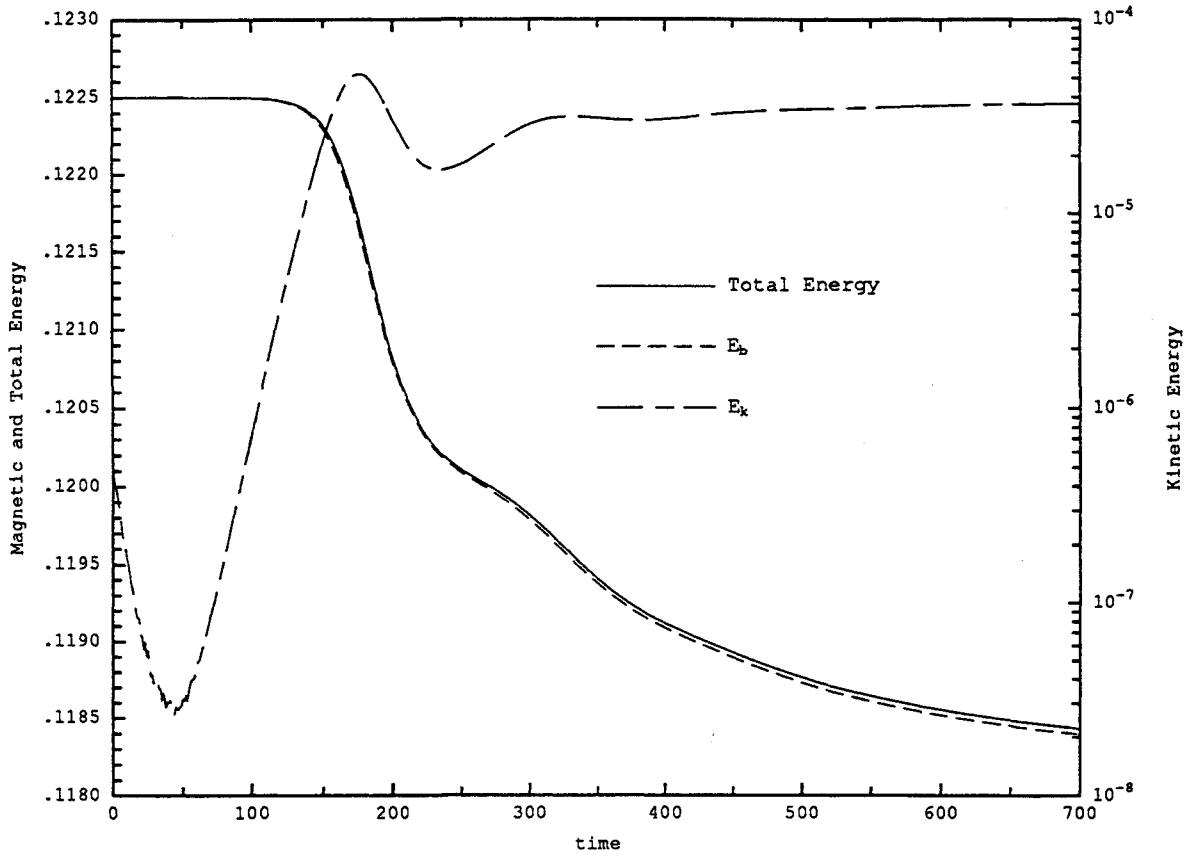

Figure 3.22: Time history of kinetic, magnetic and total energy for the same situation as shown in Fig. 3.21.

netic energies of the energetically largest helical modes. Similar to what has been shown in Figs. 3.4 and 3.5, the majority of the modes damped away in a short period. The largest mode which grows exponentially before $t = 180$ is identified as (3,1,1), the first unstable mode. After $t \simeq 200$ the (3,1,1) mode becomes nonlinearly saturated and the system evolves into a helical equilibrium which consists of only the (3,1) modes and their harmonics.

Figures 3.21 – 3.23 are the time histories of some of the global quantities plotted versus time. Shown in Figures 3.21 are the averaged current density $j_0(t)$ and E_0/η. Shown in Fig. 3.22 are the global kinetic energy, magnetic energy and the total energy. Plotted in Fig. 3.23 are the viscous, Ohmic, and the total energy dissipation rates. Initially the

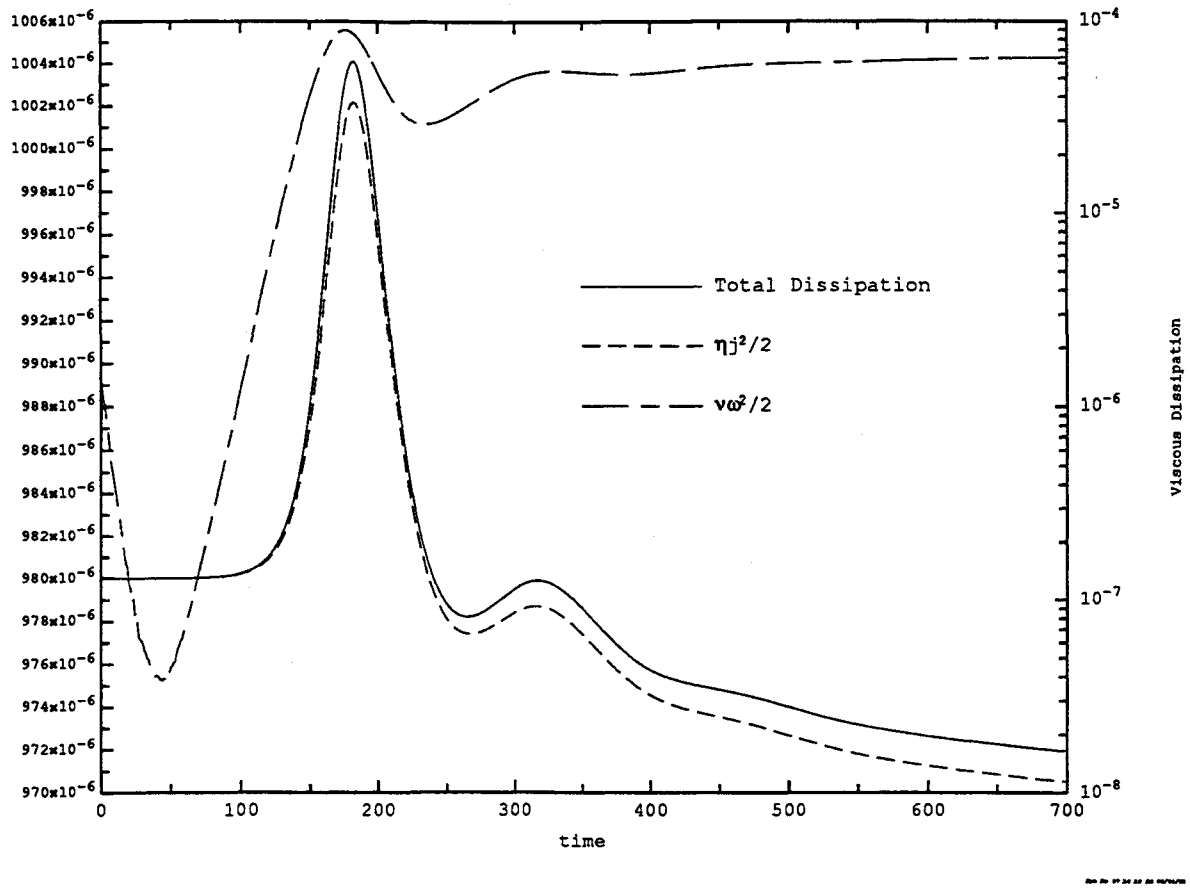

Figure 3.23: Time histories of the ohmic, viscous and total energy dissipation rates when the system undergoes a transition from the axisymmetric state to the helically deformed state.

system is in the axisymmetric equilibrium and $j_0 = E_0/\eta$. As the kinetic energy grows, the averaged current and the Ohmic dissipation rate grow *above* their axisymmetric state values and decay rapidly below the axisymmetric state values when the kinetic energy becomes saturated after $t \simeq 180$, and then approach to steady values gradually. In contrast, the magnetic energy keeps decaying in the whole process.

At the end of this high-Hartmann number run, namely at $t = 700$, a laminar steady state, dominated by the single mode (3,1), is reached. The actual pinch ratio is measured to be $\Theta = 0.278$. Similar to the steady state shown in Fig. 3.11–3.18, this steady state is also purely helically symmetric and can be characterized by a small number of

CONCLUSION:

AN ADEQUATE SET OF BOUNDARY CONDITIONS DETERMINES THE SOLUTIONS TO THE TIME-INDEPENDENT MHD EQUATIONS UNIQUELY, GIVEN A NON-ZERO RESISTIVITY AND VISCOSITY. AS LONG AS WE ARE ON THE STABLE SIDE OF THE BOUNDARIES, THERE IS NO ROLE TO PLAY FOR ANOTHER PRINCIPLE. HOWEVER, AT STABILITY BOUNDARIES, THESE STEADY SOLUTIONS MAY <u>BIFURCATE</u>. IF SO, THE MAGNETOFLUID SEEMS TO CHOOSE THE BRANCH WITH LOWER DISSIPATION, JUST ABOVE THE BIFURCATION. THE SYMMETRY MAY BE BROKEN BY THE INSTABILITY.